Construction and Building Materials 229 (2019) 116866

Contents lists available at ScienceDirect

Construction and Building Materials

journal homepage: www.elsevier.com/locate/conbuildmat

Experimental and numerical investigations on the impact resistance of SHCC-strengthened RC slabs subjected to drop weight loading

Amira B. Elnagar, Hamdy M. Afefy *, Ahmed T. Baraghith, Mohamed H. Mahmoud

Structural Engineering Dept., Faculty of Engineering, Tanta University, Tanta, Egypt

HIGHLIGHTS

- SHCC-strengthened slabs are tested under the effect of drop weight loading.
- The location of the SHCC layer at either tension or compression side is investigated.
- The effect of surface preparation condition is mainly studied.
- Impact energy of SHCC-strengthened slabs is obtained numerically using ABAQUS software.
- The most favorable surface preparation condition is identified.

ARTICLE INFO

Article history:
Received 28 April 2019
Received in revised form 7 August 2019
Accepted 1 September 2019
Available online 9 September 2019

Keywords:
Drop weight test
Ductility index
Low-velocity impact
Strain-Hardening Cementitious Composites (SHCC)
Strengthening
ABAQUS software

ABSTRACT

In this paper, a thin layer of Strain-Hardening Cementitious Composites (SHCC) is provided in either tension or compression side of RC slabs aiming to improve their impact resistance under the effect of drop weight loading. The main parameter of the current study is the condition of the contact surface between the substrate slab and the SHCC overlay that was prepared by grinding, grinding plus steel dowels or grinding plus epoxy adhesive. Accordingly, 63 RC slabs were prepared and tested under the effect of drop weight falling from three different heights; 1, 1.5 and 2 m. It was found that the SHCC strengthening layer enhanced the impact resistance of the strengthened slab when added at either tension or compression side. However, in order to attain the outermost impact resistance showing ductile performance, it is better to provide a thin layer of the SHCC at the tension side of the slab connected to the substrate slab by epoxy resin applied on pre-prepared grinded surface. Furthermore, numerical simulations based on ABAQUS software package were performed on the strengthened slabs. Their results showed good agreement with the experimental findings from the viewpoint of the kinetic energy. Besides, the impact failure loads were determined numerically for the studied slabs and compared with those obtained from incremental static loading tests.

© 2019 Elsevier Ltd. All rights reserved.

1. Introduction

Reinforced concrete structures are most likely subjected to some kinds of impact loading during their service-life. That impact loading could damage the entire structure or a specific part of it, which makes the human life at stake. The response of RC member to impact loading is divided into two stages, namely; the local response stage under the impacted point instantly after impact due to the generated stress wave at such point and the overall response stage including the free vibration of the entire member [1]. Since the impact loading affects the structural member in different way from that the static loading does, it is very essential to better understand the performance and vulnerability of reinforced concrete members under impact loading in order to mitigate the consequential catastrophic failure and protect lives as well. Therefore, several researchers have devoted their efforts to study the dynamic characteristics of RC members under impact loading. Others reported on different strengthening techniques in order to improve the overall response under impact loading.

Low energy impact response of ultra-high performance concrete (UHPC) panels for different fiber volumetric content, thickness and impactor energy had studied [2]. It was observed that the peak impact load has been increased due to the increase in the impactor energy. Similarly, the behavior of ultra-high performance fiber reinforced concrete (UHPFRC) under impact and static loading has been demonstrated [3–6]. It was concluded that 3% is the most optimum fiber volumetric ratio of the UHPFRC mixture to provide higher resistant to projectile impact.

* Corresponding author at: Structural Engineering Dept., Faculty of Engineering, Tanta University, Tanta 31511, Egypt.
E-mail address: hamdy.afefy@f-eng.tanta.edu.eg (H.M. Afefy).

https://doi.org/10.1016/j.conbuildmat.2019.116866
0950-0618/© 2019 Elsevier Ltd. All rights reserved.

In the same way, the response of thin slabs of slurry-infiltrated fibrous concrete (SIFCON) with and without reinforcement had been investigated under low-velocity impacts [7]. It was found that better performance in terms of strength and durability characteristics due to the incorporation of binary blends of silica fume and slag in SIFCON matrix was obtained. In addition, the fiber reinforced oil palm shell concrete (FROPSC) was found to exhibit a higher resistance to impact loads showing smaller crack widths [8]. Furthermore, the impact resistance of concrete slabs provided with different percentage of replacement ratios of waste plastic fibers has been investigated under the effect of drop steel ball [9]. Moreover, it was found that the pre-stressed concrete slab has better impact resistance and higher energy absorption capacity compared to those of non-pre-stressed reinforced concrete slab [10–11]. Also, the high-strength high-ductility concrete (HSHPC) slabs exhibited ductile flexural behavior along with well-distributed multiple fine cracks under impact loading [12].

The performance of newly developed soft-hard-soft (SHS) composite system under multiple impacts loading was investigated numerically and experimentally [13]. The SHS composite system exhibited minimum damage, higher energy absorption and significant improved impact resistance. A new multi-layer pavement system consisted of asphalt concrete (AC) layer reinforced with geo-grid (GST), followed by high strength concrete (HSC) layer and engineered cementitous composites (ECC) layer was developed [14]. It was observed that the new multi-layer pavement system had better blast resistance than that provided by conventional pavement system.

The interface condition between the strengthening overlays and concrete substrates is one of the most important factors that affect the strength and durability of strengthened member as well as its response to external loading. The aim of surface preparation of concrete is to remove any layers that decrease the adhesion as well as to enlarge the contact area by increasing surface roughness [15]. Different surface preparation techniques such as grinding, sand blasting, shot blasting, water jet, hand preparation and mechanical milling were considered and investigated [16–20]. The choice of the most appropriate surface preparation technique is mainly dependent on different factors including the shape of the structural member as well as the expected loading history.

Strain-hardening cementitious composites (SHCC) consist of finely grained cementitious matrices and short high-performance micro-fibers that characterized by the formation of multiple fine cracks under increasing loading up to failure. SHCC material exhibits tensile hardening behavior accompanied by the formation of fine multiple cracks [21]. The application of the strain-hardening cementitious composite (SHCC) layer as a strengthening material at either tension or compression sides proved its efficiency in enhancing the overall structural flexural behavior under incremental static loading [22–25]. In addition, it shows a considerable high tensile strain capacity, which is a main important criterion of a durable material in order to eliminate premature failures [26–29].

In the current study, in order to improve the impact resistance of RC slabs subjected to drop weight loading, a thin layer of Strain-Hardening Cementitious Composites was provided in either tension or compression side of the slab. The main parameter of the current study was the condition of the contact surface between the substrate slab and the SHCC overlay that was prepared by grinding, grinding plus steel dowels or grinding plus epoxy adhesive. Also, to validate the experimental results, numerical study based on ABAQUS software [30] has been conducted to simulate the same specimens under the effect of drop weight loading as well as incremental static loading.

2. Experimental program

2.1. Test slabs

The experimental work program was devoted to studying the response of SHCC-strengthened slabs at either tension or compression side under the effect of drop-weight falling from three different heights taking into account the surface preparation condition between the substrate slab and the SHCC overlay. For each drop-height, keeping the same surface preparation condition, three typical slabs were cast and tested in order to increase the degree of confidence in the results. Typical RC square slabs of 500 mm side length and 50 mm thickness reinforced by three smooth mild steel bars of 6 mm diameter in both directions according to the ECP-203-2018 code [31] have been prepared and cast.

Sixty three reinforced concrete slabs divided into three groups were prepared and cast. Group I was the control un-strengthened group tested under drop-weight of 13 kg falling from three different heights (1, 1.5 and 2 m). Thus, it contained 9 slab specimens. Group II consisted of 27 RC slabs strengthened in tension side by SHCC layer of 15 mm thickness applied after preparing the interface surface of the substrate slabs. Three configurations of the surface preparation were considered; namely, grinding, grinding plus epoxy adhesive and grinding plus steel shear dowels as depicted in Figs. 1 and 2. Group III consisted of similar 27 RC slabs as those of group II, however, the SHCC layers were provided in compression side as depicted in Fig. 1 and as summarized in Table 1.

It is worth mentioning that, the SHCC layers were reinforced by welded wire mesh of 3 mm diameter and 50 mm spacing in both directions. That is to have better crack distribution in the SHCC layers in addition to enable the SHCC to exhibit more softening plateau [22].

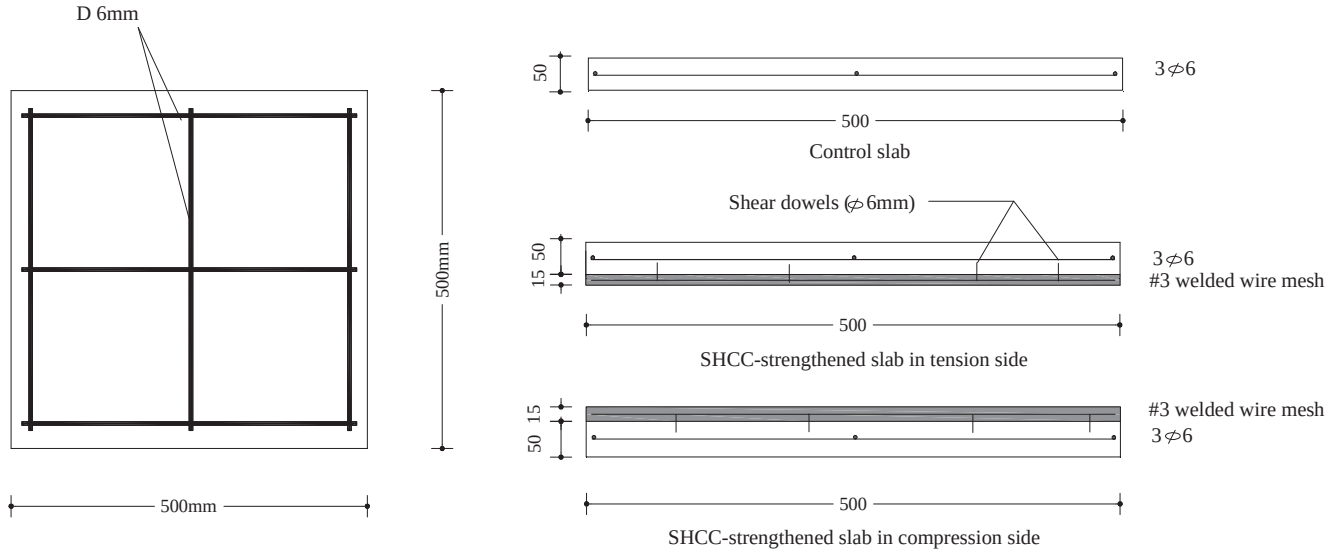
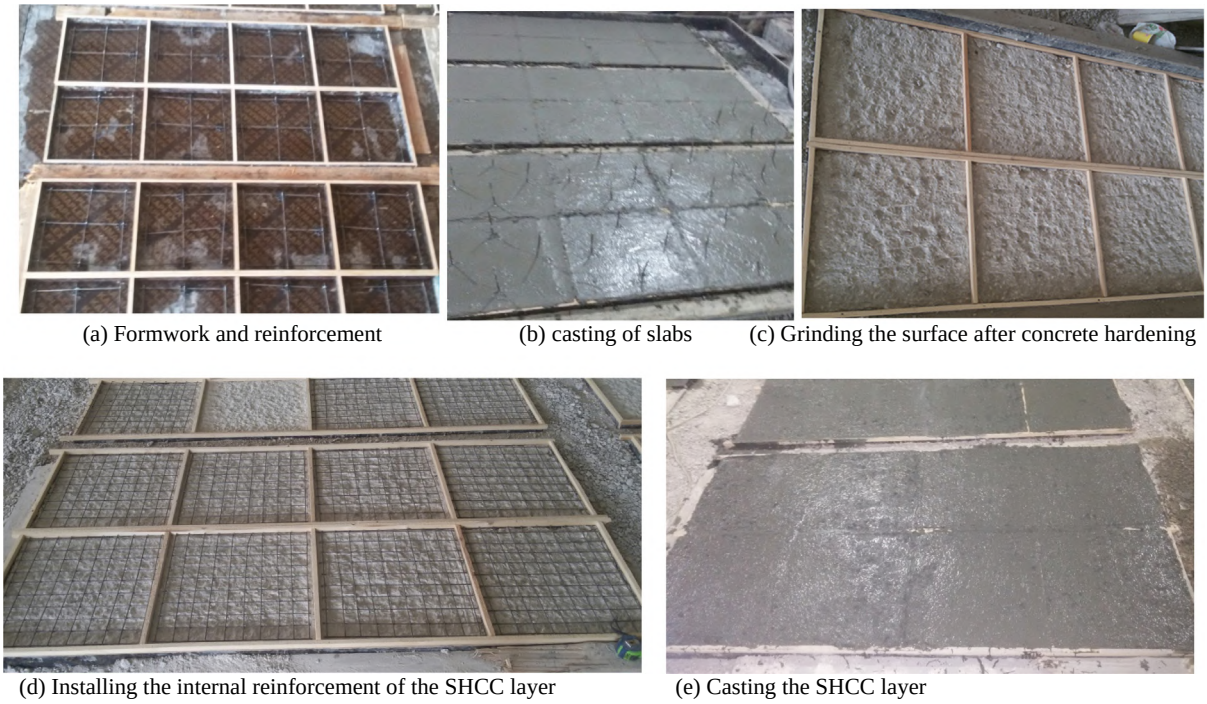


Fig. 1. Typical concrete dimensions and reinforcement.



(a) Formwork and reinforcement (b) casting of slabs (c) Grinding the surface after concrete hardening

(d) Installing the internal reinforcement of the SHCC layer (e) Casting the SHCC layer

Fig. 2. Fabrication and preparation of test slabs.

Table 1
Test specimens.

Group No.	Strengthened side	Slab ID	Surface preparation type	H, m	Slab Rft in both directions	No. of typical specimens
GI	Un-strengthened	SC1	NA	1	3Ø6	3
		SC1.5		1.5	3Ø6	3
		SC2		2	3Ø6	3
GII	Tension	STG1	Grinding	1	3Ø6	3
		STGE1	Grinding + Epoxy	1	3Ø6	3
		STGD1	Grinding + Dowels	1	3Ø6	3
		STG1.5	Grinding	1.5	3Ø6	3
		STGE1.5	Grinding + Epoxy	1.5	3Ø6	3
		STGD1.5	Grinding + Dowels	1.5	3Ø6	3
		STG2	Grinding	2	3Ø6	3
		STGE2	Grinding + Epoxy	2	3Ø6	3
		STGD2	Grinding + Dowels	2	3Ø6	3
GIII	Compression	SCG1	Grinding	1	3Ø6	3
		SCGE1	Grinding + Epoxy	1	3Ø6	3
		SCGD1	Grinding + Dowels	1	3Ø6	3
		SCG1.5	Grinding	1.5	3Ø6	3
		SCGE1.5	Grinding + Epoxy	1.5	3Ø6	3
		SCGD1.5	Grinding + Dowels	1.5	3Ø6	3
		SCG2	Grinding	2	3Ø6	3
		SCGE2	Grinding + Epoxy	2	3Ø6	3
		SCGD2	Grinding + Dowels	2	3Ø6	3

H = drop-height; Rft = reinforcement.

All substrate slabs were cast at the same time using ready-mix concrete patch having target 28-day cube strength of 30 MPa, The averaged compressive strength based on 18 standard cubes of 150 mm side length collected at different times of casting and testing was determined to be 32.4 MPa, while the average tensile split strength based on indirect split cylinder test of 9 standard cylinders of 150 mm diameter and 300 mm height was about 3.1 MPa.

The used SHCC material consisted of Type-I cement, natural sand, silica fume, super-plasticizers, expansion agent, polypropylene fiber and clean tap water with proportions as given in Table 2. High strength polypropylene (PP) short fibers of 0.012 mm diameter and 6 mm length were selectively chosen considering fiber volumetric ratio of 1.5%. The mass density, tensile strength and the elastic modulus of the used PP fibers according to the manufacturer's data sheet were 910 kg/m^3, 625 MPa and 3.7 GPa, respectively. A horizontal shear mixer has been used in order to mix the SHCC material. Then, the SHCC patch was poured on the pre-prepared substrate surfaces.

For the SHCC material, the averaged indirect tensile strength based on split cylinder test of 6 standard cylinders and the average compressive strength based on 12 standard cubes were determined to be 6.6 MPa and 65 MPa, respectively. Fig. 3 shows typical direct tensile stress–strain curve for the SHCC material [21].

After demolding, all control and the SHCC-strengthened slabs were cured by water for 14 days then left till the testing day after 28 days of casting.

For the reinforcing steel bars of 6 mm diameter, the average yield strength, tensile strength and Young's modulus were about 270 MPa, 530 MPa and 205 GPa, respectively. While, the average yield strength for the 3 mm diameter smooth bars forming the orthogonal mesh provided in the SHCC layer was about 320 MPa.

2.2. Test setup and procedures

Fig. 4 show schematic diagram of the used setup for the drop-weight impact test. A free falling mass of about 13 kg was dropped onto the top surface of the

Table 2
Mix proportions of SHCC for one cubic meter (kg).

Water	Cement	Silica fume	Expansion agent	Sand	Super plasticizer	Air reducer	PP Fiber (6 mm)
292	1243	223	20	149	14.9	2.98	14.6

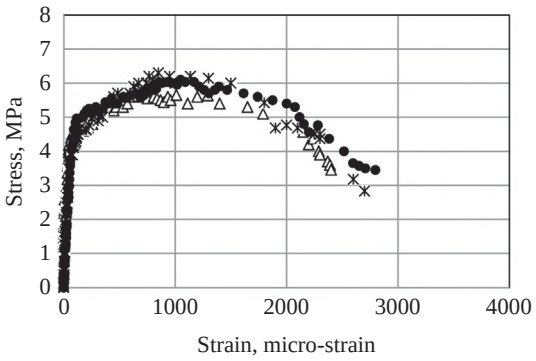


Fig. 3. Typical axial tensile stress-strain relationship for SHCC material.

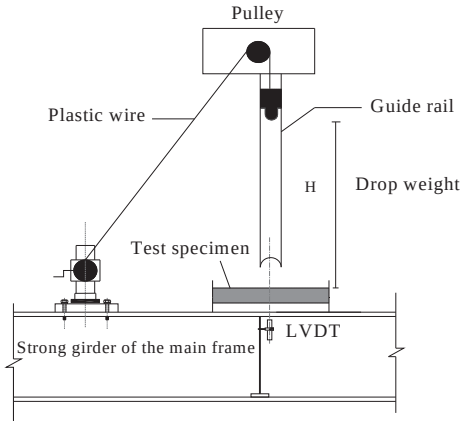


Fig. 4. Drop-weight impact test setup and supporting system.

tested slabs at central point from three different heights; 1, 1.5 and 2 m. The head of the drop weight was prepared to have a hemispherical tip with a radius of 50 mm in order to eliminate any stress concentration at the point of impact. In addition, a guide rail was used in order to guide the falling weight to the same striking point. The test slabs are clamped at their four corners using a special tie-down steel frame in order to prevent them from uplift. The mid-span deflection-time responses of the test slabs were measured by LVDT mounted at the central point of the slab. All output data are recorded using a digital dynamic data acquisition system KYOWA model PCD-300A with sampling rate of 5 kHz. In addition, crater diameter and penetration depth were also measured, if any.

3. Test results and discussion

Each slab was subjected to repeated impacts due to drop-weight of about 13 kg released from the assigned drop-height where the numbers of blows corresponding to the first visible crack and the complete collapse were recognized and recorded.

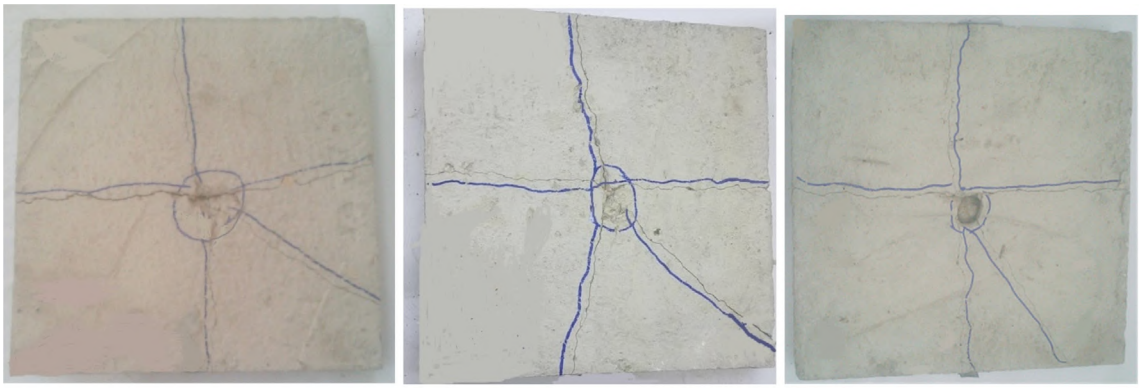
3.1. Crack patterns and failure modes

Fig. 5 shows the developed cracks and failure zone at the bottom (rear face) and the top (impacted face) of un-strengthened slabs of group I corresponding to the three drop-heights. It can be noticed that the final crack pattern at failure was approximately the same for the three drop-heights, however, the number of blows requited to trigger the complete failure decreased with the increase of the drop-height, which confirmed with other experimental findings [32,33]. The numbers of blows corresponding to failure of un-strengthened slabs were 18, 10 and 6, respectively, for the drop-heights 1, 1.5 and 2 m as summarized in Table 3. It was noticed that the cracking patterns at both impacted and rear faces were approximately the same which were radial cracks started from the central point as depicted in Fig. 5. Regarding the commencement of visible tensile crack, the slab SC1 started to develop visible cracks after the third blow, while both slabs SC1.5 and SC2 exhibited visible cracks after the second blow. The most important observation was that the cracking pattern was approximately the same along the entire loading history till the complete collapse; however, the crack width was noticed to be increased with the increase of the number of blows. In addition, under the impacted point, concrete was spalled out at small region as depicted in Fig. 5.

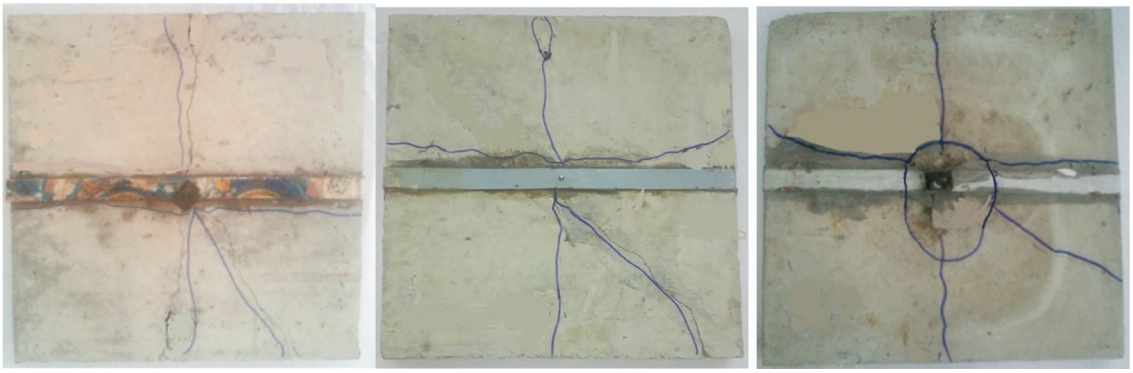
Figs. 6–8 show the crack patterns at failure for all slabs of group II that were strengthened by thin layer of SHCC applied at the tension side for the drop-heights 1, 1.5 and 2 m, respectively. It can be noticed that the surface preparation condition which was grinding, grinding plus epoxy adhesive or grinding plus steel shear dowels did not affect the final cracking pattern or the failure mode. However, it affected the number of sustained blows till the typical flexural failure modes were exhibited for all test slabs. The failure was characterized by spalling of concrete at the impacted point with crater diameters and penetration depths as listed in Table 3, while the tension side was characterized by multiple orthogonal cracks perpendicular to the slab edges having smaller crack widths compared to those of the relevant control slabs of group I.

For slabs impacted by drop-weight released from drop-height of 1 m, the strengthened slabs adopted the grinding plus epoxy adhesive sustained the highest number of blows till the complete collapse, while the strengthened slabs prepared by the grinding technique only sustained the lowest numbers of blows. The numbers of sustained blows were 63, 84, and 72, respectively for slabs prepared by grinding (G), grinding plus epoxy adhesive (GE) and grinding plus steel shear dowels (GD). These numbers are corresponding to 3.5, 4.7 and 4 times the numbers caused failure for the control slab SC1. That could be attributed to the increased overall depth (65 mm compared to 50 mm), which resulted in increased stiffness and strength of the strengthened slabs along with the enhanced tensile characteristics of the SHCC material that enabled the impacted slab to absorb the impact energy showing multiple hair cracks. Moreover, it was found that using synthetic fibers such as polypropylene in concrete improved its impact resistance [34–37]. Thus, the surface preparation implemented by grinding plus epoxy adhesive (GE) showed the most enhanced results among the adopted techniques.

Increasing the drop-height to 1.5 m or 2 m did not affect the failure pattern for the SHCC-strengthened slabs at the tension side as depicted in Figs. 7 and 8; however it decreased the number of sustained blows till complete failure of the slabs as summarized in Table 3. The numbers of sustained blows were 50, 73, and 60, respectively for slabs STG1.5, STGE1.5 and STGD1.5. These numbers are corresponding to 5, 7.3 and 6 times the numbers caused failure for the control slab SC1.5. Similarly, the numbers of sustained blows were 41, 49, and 37, respectively for slabs STG2, STGE2 and STGD2. These numbers are corresponding to 6.8, 8.2 and 6.2 times the numbers caused failure for the control slab



(a) Slab SC1 (top) (N=18) (b) Slab SC1.5 (top) (N=10) (c) Slab SC2 (top) (N=6)



(d) Slab SC1 (bottom) (N=18) (e) Slab SC1.5 (bottom) (N=10) (f) Slab SC2 (bottom) (N=6)

Fig. 5. Developed cracks and failure zone at the bottom and the top surfaces of un-strengthened slabs.

Table 3
Test results of all groups.

Group No.	Slab ID	H, m	N_f	Δ_{max} mm	D, mm	d, mm
GI	SC1	1	18	2.65	NA	NA
	SC1.5	1.5	10	3.39	NA	NA
	SC2	2	6	4.00	NA	NA
GII	STG1	1	63	1.33	100	0.85
	STGE1	1	84	2.05	90	0.7
	STGD1	1	72	1.84	80	1
	STG1.5	1.5	50	1.92	100	0.75
	STGE1.5	1.5	73	2.16	100	1
	STGD1.5	1.5	60	2.14	80	0.5
	STG2	2	41	2.22	100	0.9
	STGE2	2	49	2.33	60	0.5
	STGD2	2	37	2.41	85	0.9
GIII	SCG1	1	49	2.49	NA	NA
	SCGE1	1	52	2.45	NA	NA
	SCGD1	1	63	1.90	NA	NA
	SCG1.5	1.5	27	3.00	NA	NA
	SCGE1.5	1.5	31	2.65	NA	NA
	SCGD1.5	1.5	43	2.24	NA	NA
	SCG2	2	15	3.37	NA	NA
	SCGE2	2	16	2.42	NA	NA
	SCGD2	2	19	2.83	NA	NA

H = drop-height; N_f = number of blows till complete failure; Δ_{max} = maximum deflection; D = crater diameter; d = penetration depth; NA = not applicable.

SC2. It could be noticed that, increasing the drop-height enabled the strengthened slabs to sustain more impact energy compared to the relevant un-strengthened slab. For instance, the slabs adopting the most promising surface preparation technique STGEs, the numbers of sustained blows till complete failure of slabs STGE1, STGE1.5 and STGE2 were 4.7, 7.3 and 8.2 respectively, times that of the opponent slabs SC1, SC1.5 and SC2.

For all slabs strengthened by SHCC layer at the tension side subjected to drop weights released from different heights and adopting different surface preparation techniques, no visible detachment between both the substrate slab and the SHCC layer after the complete collapse of slabs was noticed.

Dissimilar to the slabs strengthened in tension side by SHCC layers, both the drop-height and the surface preparation

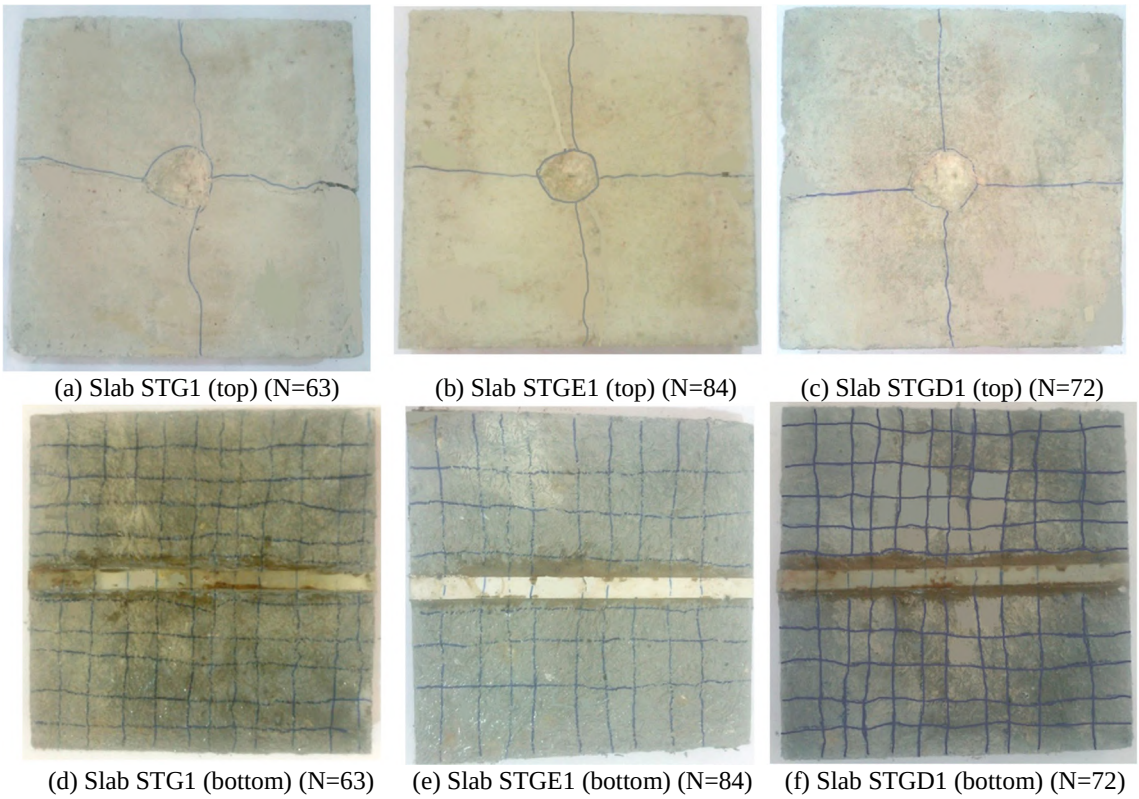


Fig. 6. Developed cracks and failure zone the at top and the bottom surfaces of SHCC-strengthened slabs at tension side subjected to drop weight from 1 m height.

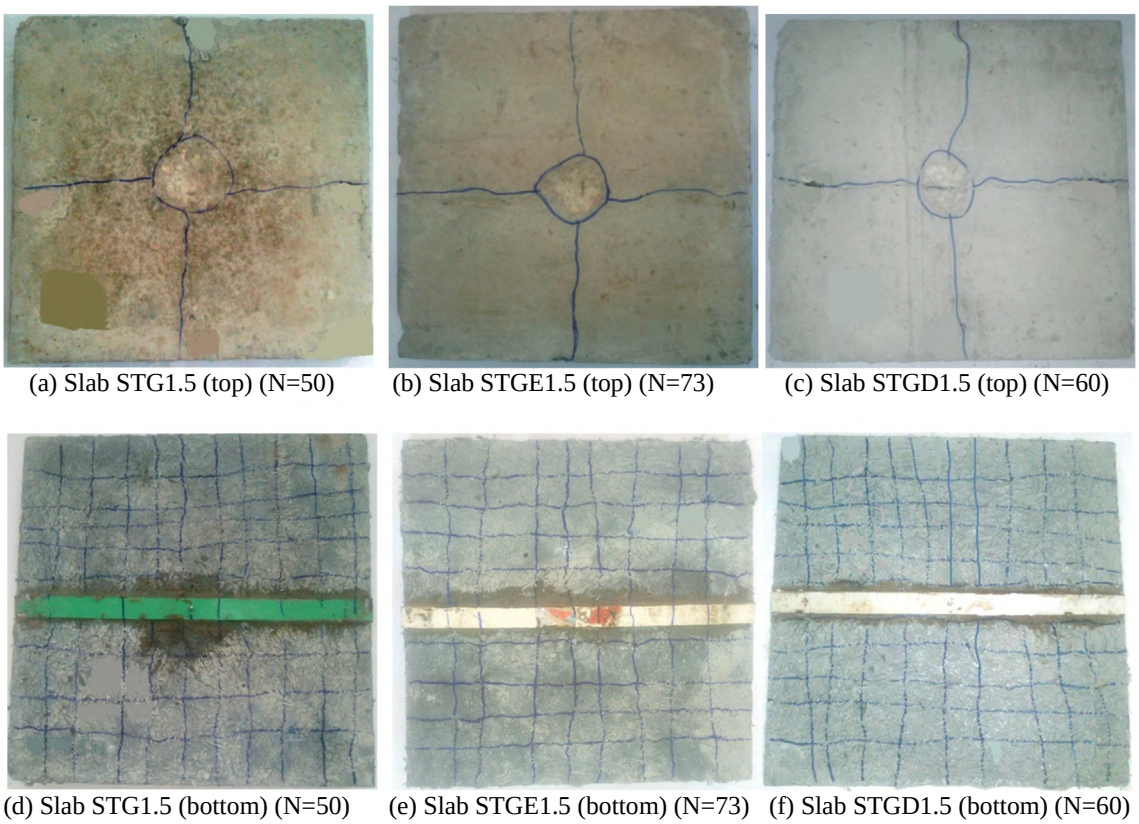
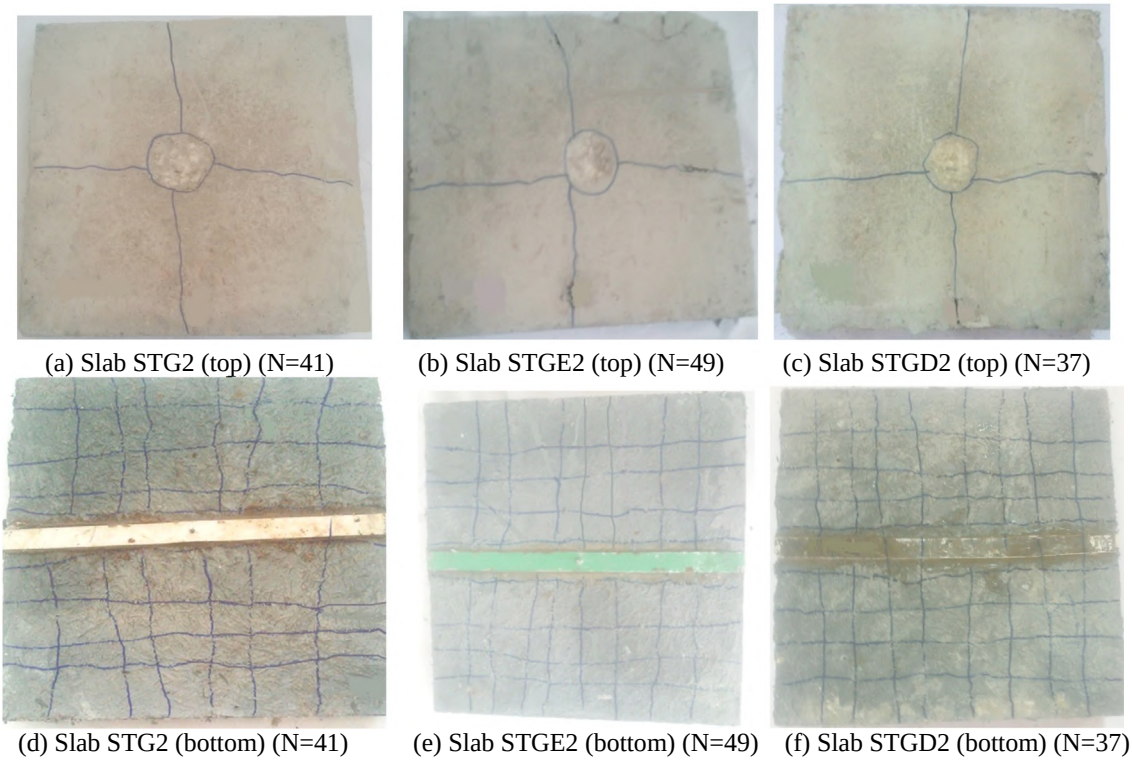


Fig. 7. Developed cracks and failure zone at the top and the bottom surfaces of SHCC-strengthened slabs at tension side subjected to drop weight from 1.5 m height.



(a) Slab STG2 (top) (N=41) (b) Slab STGE2 (top) (N=49) (c) Slab STGD2 (top) (N=37)

(d) Slab STG2 (bottom) (N=41) (e) Slab STGE2 (bottom) (N=49) (f) Slab STGD2 (bottom) (N=37)

Fig. 8. Developed cracks and failure zone at the top and the bottom surfaces of SHCC-strengthened slabs at tension side subjected to drop weight from 2 m height.

techniques affected the cracking patterns at failure of all slabs provided by SHCC layer at the compression side as depicted in Figs. 9–11. Similarly, the less significant technique was that based on grinding the interface surface only. On contrary, the most significant technique was that based on grinding plus steel shear dowels for slabs strengthened by SHCC layer at the compression side.

For the strengthened slabs by SHCC layer at the compression side, all slabs sustained lower numbers of blows till complete failure compared to relevant slabs strengthened at the tension side taking into account the surface preparation conditions. This can be attributed to that the tension side of such slab was made of normal strength concrete which is brittle in tension and leak of tension soften plateau that provided by the SHCC material. In addition, the SHCC is more ductile than the normal strength concrete which exhibits more deformation when dissipated the impact energy where that deformation cannot be fully delivered to the substrate slab by the epoxy but could by delivered more effectively through the steel dowels, which have sufficient ductility. Hence, the technique based on grinding plus steel shear dowels (GD) showed more impact resistance than that exhibited by the technique based on grinding plus epoxy (GE). That happened for the three drop-heights.

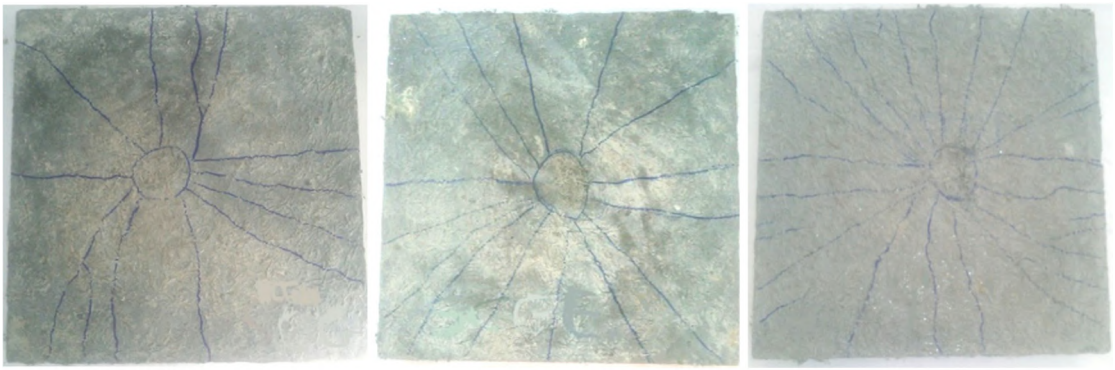
Table 3 summarizes the sustained numbers of blows for all specimens of group III. It can be noticed that the sustained numbers of blows are corresponding to 2.7, 2.9, and 3.5, respectively for slabs SCG1, SCGE1 and SCGD1 times that caused failure for control slab SC1. For the drop height of 1.5 m, the sustained numbers of blows are 2.7, 3.1, and 4.3, respectively for slabs SCG1.5, SCGE1.5 and SCGD1.5 times that caused failure for control slab SC1.5. Similarly, the sustained numbers of blows are 2.5, 2.7, and 3.2, respectively, for slabs SCG2, SCGE2 and SCGD2 times that caused failure for control slab SC2.

Fig. 12 shows comparison among the sustained numbers of blows for all test slabs. It can be observed that strengthening RC slabs by thin layer of SHCC at tension side is better than that strengthening such slabs by the same layer at the compression side. In addition, when strengthening the slab at tension side, the preparation technique based on grinding plus epoxy adhesive showed the most significant impact resistance. On the other hand, when the SHCC was used at the compression side, it is better to use steel dowels plus grinding in order to obtain the most effective impact performance.

For the current study, it was difficult to define the failure accurately. Therefore, certain criteria were set. First, one person was in charge for stopping the test at failure in order to have the same personal error. Second, for un-strengthened slabs, the test was stopped after the crushing of the entire slab and the failure state was considered as the last event before scattering the slab. For strengthened slabs by SHCC layer at either tension or compression side, the SHCC layer kept the integrity of the strengthened slabs at either tension or compression side. Thus, the SHCC-strengthened slabs did not break, however, the substrate slabs showed severe cracks and local damages at the tension side when the added SHCC was provided at the compression side. Accordingly, the strengthened slabs at the compression sides were considered to be failed after developing local failure on the substrate slab. Thus the failure state was considered as the last drop event before such local damage. On the other hand, the strengthened slabs at the tension side were considered to be failed at the last event before concrete crushing at the compression side.

3.2. Maximum mid-span deflection-time history response

The mid-span deflection-time history response of the slab after each impact event was measured by LVDT displacement sensor MTN/ EDX050 attached at the central point of the slab. After each impact event, the LVDT was checked for misalignment and set to zero and then the following hit was applied. Accordingly, the measured mid-span deflection-time history response represented the event deflection variation and did not demonstrate the accumulation of residual mid-span deflection from prior impacts owing to the inelastic behavior of both RC and SHCC material.

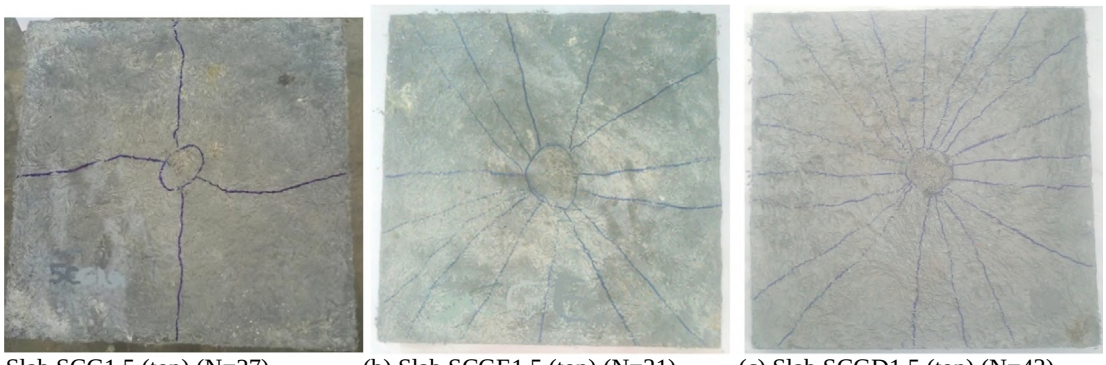


(a) Slab SCG1 (top) (N=49) (b) Slab SCGE1 (top) (N=52) (c) Slab SCGD1 (top) (N=63)



(d) Slab SCG1 (bottom) (N=49) (e) Slab SCGE1 (bottom) (N=52) (f) Slab SCGD1 (bottom) (N=63)

Fig. 9. Developed cracks and failure zone at the top and the bottom surfaces of SHCC-strengthened slabs at compression side subjected to drop weight from 1 m height.

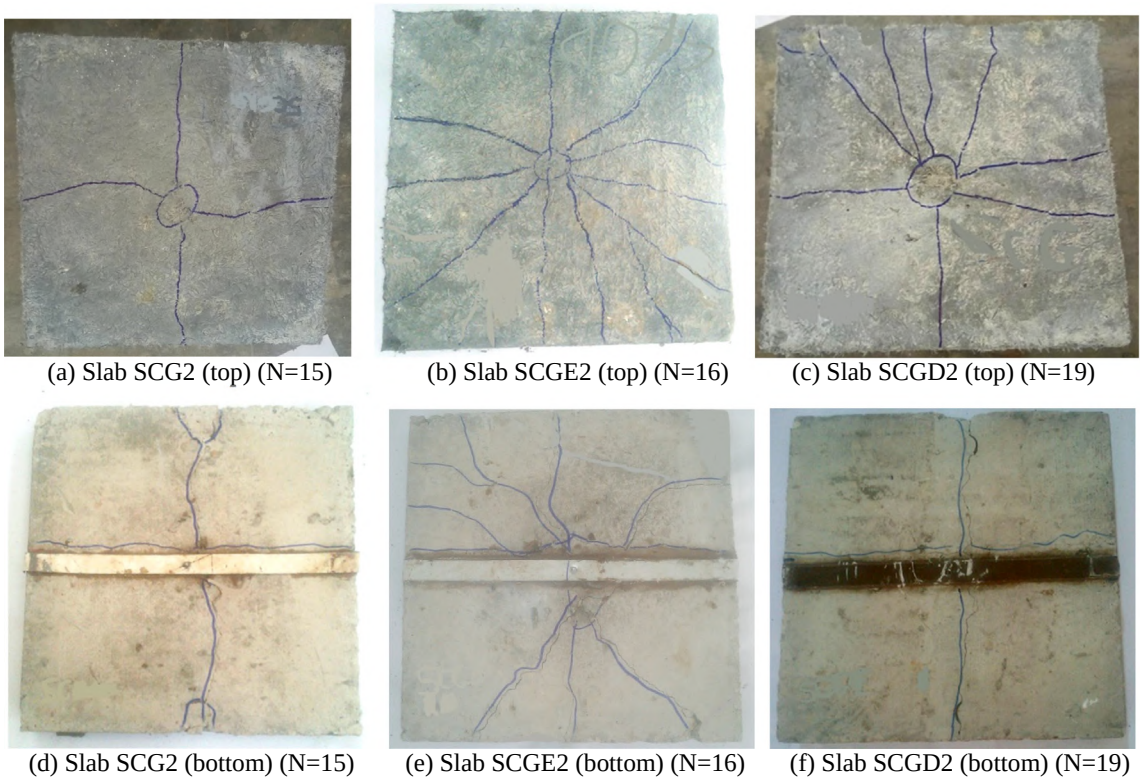


(a) Slab SCG1.5 (top) (N=27) (b) Slab SCGE1.5 (top) (N=31) (c) Slab SCGD1.5 (top) (N=43)



(d) Slab SCG1.5 (bottom) (N=27) (e) Slab SCGE1.5 (bottom) (N=31) (f) Slab SCGD1.5 (bottom) (N=43)

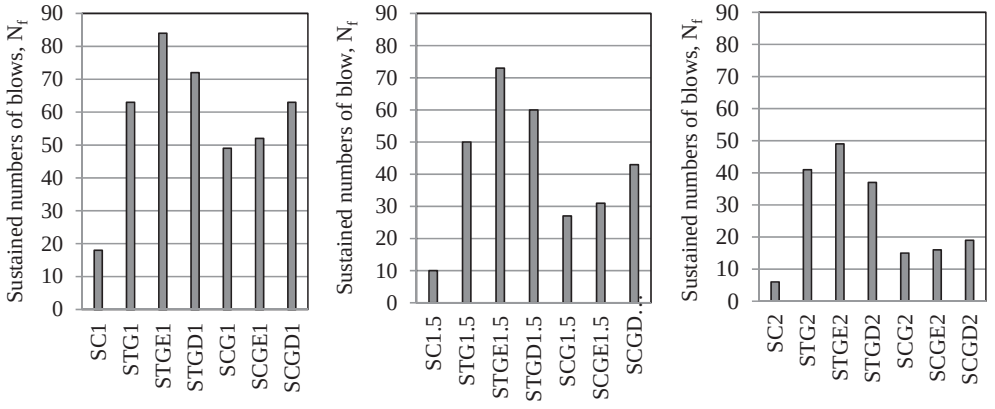
Fig. 10. Developed cracks and failure zone at the top and the bottom surfaces of SHCC-strengthened slabs at compression side subjected to drop weight from 1.5 m height.



(a) Slab SCG2 (top) (N=15) (b) Slab SCGE2 (top) (N=16) (c) Slab SCGD2 (top) (N=19)

(d) Slab SCG2 (bottom) (N=15) (e) Slab SCGE2 (bottom) (N=16) (f) Slab SCGD2 (bottom) (N=19)

Fig. 11. Developed cracks and failure zone at the top and the bottom surfaces of SHCC-strengthened slabs at compression side subjected to drop weight from 2 m height.



(a) H=1 m (b) H=1.5 m (c) H=2 m

Fig. 12. Comparison among the sustained numbers of blows for all test slabs.

For each impact event, the maximum amplitude was recorded and then traced against the drop number for each drop-height as depicted in Fig. 13 for all un-strengthened control slabs. For each drop-height, the RC slab was noticed to exhibit progressively increased peak amplitude of the maximum deflection till a certain drop number, and then it showed some declination of the manifested deflection till the complete collapse of the slab specimen. This can be attributed to that at the elastic slate of the slab; the developed deflection at the impact event was restored after the impact effect disappeared. After cracking of the concrete, some plastic deformation was developed and retained before the following impact event. When the LVDT reading set to zero before the start of the next impact, some permanent plastic deflection was deducted. Hence, the apparent mid-span deflection was shown to be reduced since the recorded deflection represents the event deflection not the accumulative one. In addition, increasing the drop-height resulted in the increase the manifested mid-span deflection and decrease the number of blows required to cause the complete collapse of the slab compared to those of smaller drop-height.

In a similar way, the maximum amplitude was recorded and then traced against the drop number for each drop-height as depicted in Fig. 14 for all SHCC-strengthened slabs at tension side. It can observed that, after reaching the peak point, the rate of declination of the impact event was reduced compared to that of control un-strengthened slabs. This could be attributed to the strain-hardening characteristics of the SHCC material at the tension side. Among the adopted preparation techniques for

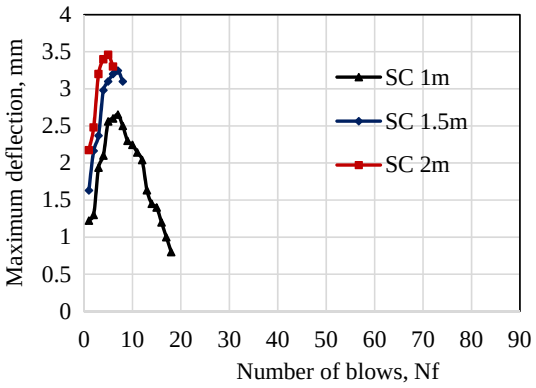


Fig. 13. Maximum mid-span deflection versus the number of blows for all drop-heights of all control un-strengthened slabs of group I.

the interface surface, the adopted technique based on the grinding plus the epoxy adhesive (GE) showed the outstanding impact resistance showing lower declination of the event deflection along with the increased numbers of sustained blows till complete failure.

On contrary, applying the SHCC layer at the compression side could not enhance the maximum event deflection since the rate of declination was shown to be high compared to that of the control slab. In addition, the preparation technique based on the grinding plus steel dowel (GD) showed the most promising technique for the current strengthening configuration as depicted in Fig. 15. The most significant observation was that the developed maximum deflections of strengthened slabs at the compression side were higher than those developed by the opponent slabs strengthened at the tension side.

3.3. Impact energy and ductility index

The drop-weight impact energy corresponding to first visible flexural crack at the tension side or complete failure of test slabs was calculated by Eq. (1) [8].

$$E_{impact} = Nmgh \quad (1)$$

where N is the number of blows corresponding to either the first crack (N_{fc}) or complete failure (N_f), m is the mass of the drop weight = 13 kg, g is the acceleration of gravity = 9.8 m/s^2, h is the drop-height = 1, 1.5 or 2 m. For a specific test, where the mass, acceleration of gravity and the drop-height are the same, the ratio of number of blows to cause failure (N_f) to the number of blows corresponding to the first crack is defined as the impact ductility index (μ_i) as expressed by Eq. (2) [26].

$$\mu_i = \frac{N_f}{N_{fc}} \quad (2)$$

Table 4 summarizes the impact energies corresponding to the first visible crack and complete failure along with the impact ductility indices for all un-strengthened and SHCC-strengthened slabs. It can be noticed that all un-strengthened and SHCC-strengthened slabs started to show visible cracks after the third blow for the drop-height of 1 m, while the number of blows corresponding to the first visible crack became two for both the drop-heights 1.5 and 2 m.

For the un-strengthened slabs of group I, increasing the drop-height from 1 m to 2 m resulted in decrease the impact ductility index by 50%. Providing a thin layer of SHCC at tension side enabled the strengthened slabs to exhibit extremely higher ductility indices compared to those of the control slabs. Increasing the drop-height from 1 m to 1.5 m resulted in increase the ductility indices by about 19, 30 and 25%, respectively, corresponding to the surface preparation techniques; grinding (G), grinding plus epoxy (GE), and grinding plus steel dowels (GD). On the other hand, increasing the drop-height further to 2 m resulted in decrease the ductility indices by about 2.5, 12.5, and 23%, respectively for surface conditions G, GE and GD. However, the ductility indices for all strengthened slabs of group II were higher than those of group I. But, the most significant results were exhibited by slabs adopted GE surface preparation technique. The ductility indices for slabs STGE1, STGE1.5 and STGE2 were about 4.7, 7.3 and 8.2 times those of slabs SC1, SC1.5 and SC2, respectively.

Based on the results listed in Table 4, it can be observed that the ductility indices for all slabs strengthened in compression side were lower than those exhibited by the opponent slabs strengthened in the tension side. The percentages of ductility indices for slabs strengthened in compression side to those strengthened at tension side were 0.78, 0.62, 0.88, 0.54, 0.42, 0.72, 0.37, 0.35 and 0.51, respectively, for surface preparation condition along with drop-heights of G1, GE1, GD1, G1.5, GE1.5, GE1.5, G2, GE2 and GD2. However, for this strengthening configuration, the surface preparation based on grinding plus steel dowels (GD) showed the most significant enhancement in the developed ductility. Thus, the ductility indices for slabs SCGD1, SCGD1.5 and SCGD2 were about 3.5, 4.3 and 3.2 times those of slabs SC1, SC1.5 and SC2, respectively.

4. Finite element simulation

In order to simulate the actual dynamic behavior for the tested slabs considering the three phases; un-strengthened,

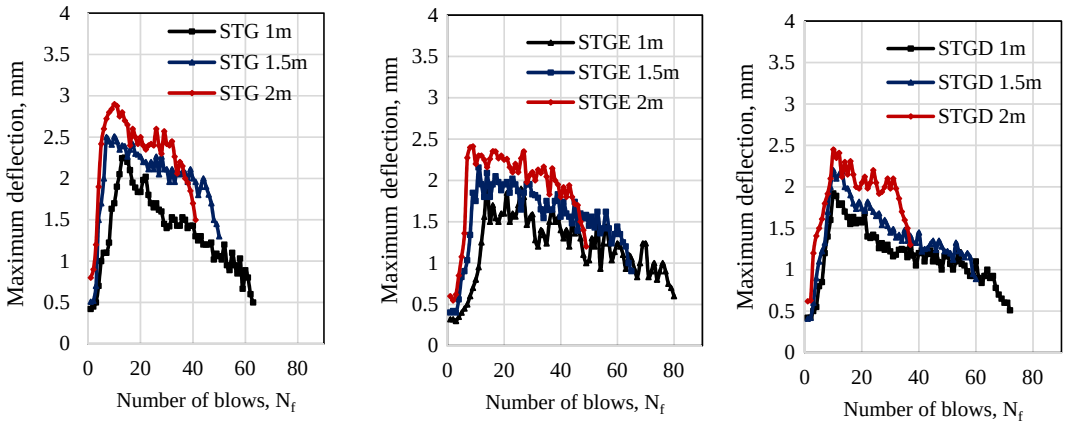


Fig. 14. Maximum mid-span deflection versus the number of blows for all drop-heights of all strengthened slabs of group II.

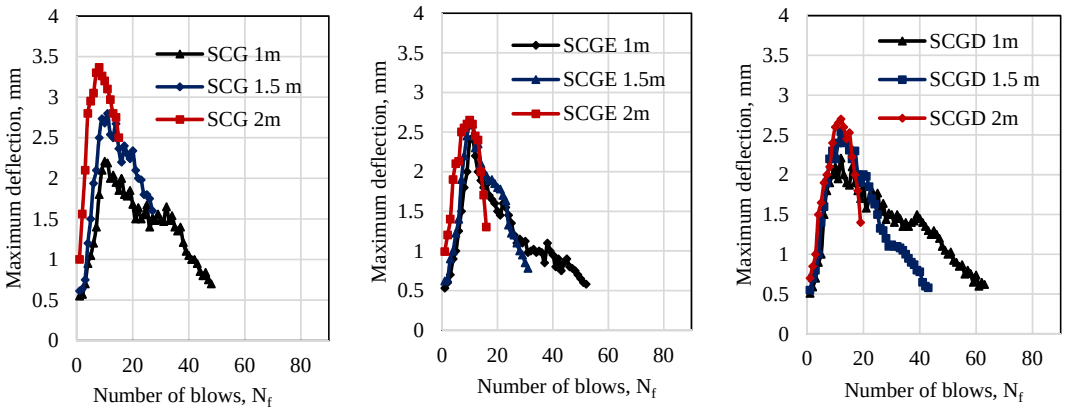


Fig. 15. Maximum mid-span deflection versus the number of blows for all drop-heights of all strengthened slabs of group III.

Table 4
Drop-weight impact energy.

Group No.	Slab ID	H, m	N_{fc}	N_f	Impact energy (first crack), J	Impact energy (failure), J	μ_i
GI	SC1	1	3	18	381	2286	6
	SC1.5	1.5	2	10	382	1910	5
	SC2	2	2	6	510	1530	3
GII	STG1	1	3	63	381	8001	21
	STGE1	1	3	84	381	10,668	28
	STGD1	1	3	72	381	9144	24
	STG1.5	1.5	2	50	382	9550	25
	STGE1.5	1.5	2	73	382	13,943	36.5
	STGD1.5	1.5	2	60	382	11,460	30
	STG2	2	2	41	510	10,455	20.5
	STGE2	2	2	49	510	12,495	24.5
	STGD2	2	2	37	510	9435	18.5
GIII	SCG1	1	3	49	381	6223	16.3
	SCGE1	1	3	52	381	6604	17.3
	SCGD1	1	3	63	381	8001	21
	SCG1.5	1.5	2	27	382	5157	13.5
	SCGE1.5	1.5	2	31	382	5921	15.5
	SCGD1.5	1.5	2	43	382	8213	21.5
	SCG2	2	2	15	510	3825	7.5
	SCGE2	2	2	16	510	4080	8.5
	SCGD2	2	2	19	381	4845	9.5

N_{fc} = number of blows corresponding to the first visible crack; N_f = number of blows till complete failure; μ_i = impact ductility index.

SHCC-strengthened slabs at tension sides and SHCC-strengthened slabs at compression sides, three dimensional (3D) finite element models based on ABAQUS software package were employed as depicted in Fig. 16 [31]. 3D modeling would enable accurate simulation of tested specimens under drop weight impact load since stresses and strains distributions are in three dimensional particularly at the impacted zone [38]. ABAQUS/Explicit is one product of ABAQUS software that has been designed particularly to solve discontinuous nonlinear dynamic problems such as impact and blast loads [30] It uses explicit integration in which the equations of motion are satisfied at the current time step, and extrapolated to determine the solution of the next time step where the values of nodal displacements, velocities and accelerations at the end of any time increment are merely based on the same quantities as at the beginning of the current time step, which explains why this method is considered explicit. Consequently, explicit analysis requires less computational time since there is no need to form the global stiffness matrix for the model [39].

In order to simulate concrete slabs and SHCC layers, 8-nodes reduced-integration solid elements having one integration point were adopted, while embedded truss elements were used to simulate the internal steel reinforcing bars. Linear interpolation elements with reduced integration have been found to be very efficient compared to fully integrated element in modeling contact

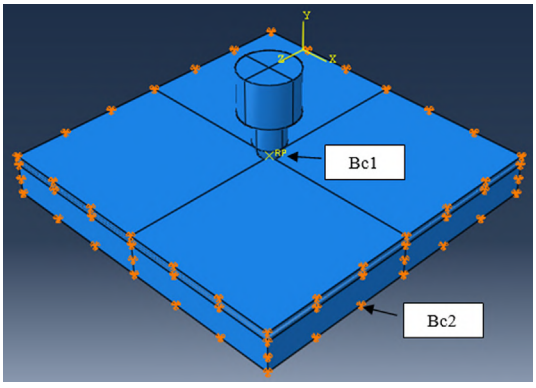


Fig. 16. 3D representation of the projectile - plate impact specimen.

impact as recommended by [38]. This could be attributed to that first-order element has a lumped mass formulation which is suitable for explicit dynamic analysis. Thus, first-order reduced-integration elements have been commonly used in most of the previous dynamic numerical studies [40–42].

Property assignment for concrete material as well as the SHCC material can be integrated into 4 basic inputs: (a) Elastic property

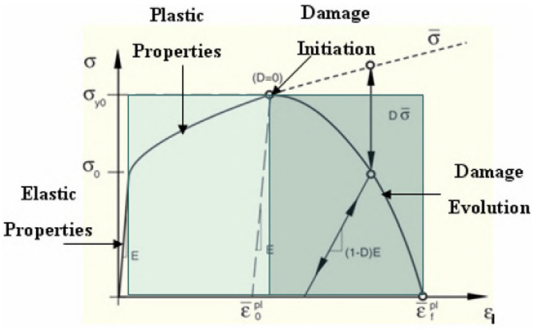


Fig. 17. Material Property Inputs for simulated stress- strain curve.

inputs (b) Plastic property inputs (c) Damage initiation input (d) Damage evolution inputs. ABAQUS/Explicit allows for individual models and their combinations to be simultaneously used for any of the listed inputs. The elastic and plastic inputs can be directly derived from stress-strain relationship for the selected materials. As depicted in Fig. 17, for any ideal material the stiffness steadily increases till it reaches a maximum point beyond which there is a steady degradation in its value. The maximum point is considered as the material damage initiation stage (when damage parameter considered for erosion, $D = 0$). The progress from maximum

Table 5
Comparison between experimental and numerical results of Impact energy.

Group No.	Slab ID	Impact energy (Model), J	Impact energy (Test), J	Mode/ test
GI	SC1	3092	2286	0.74
	SC1.5	2873	1910	0.66
	SC2	1704	1530	0.90
GII	STG1	10,087	8001	0.79
	STGE1	10,087	10,668	1.06
	STGD1	10,087	9144	0.91
	STG1.5	13,479	9550	0.71
	STGE1.5	13,479	13,943	1.03
	STGD1.5	13,479	11,460	0.85
	STG2	13,502	10,455	0.77
	STGE2	13,502	12,495	0.93
	STGD2	13,502	9435	0.70
GIII	SCG1	8503	6223	0.73
	SCGE1	8503	6604	0.78
	SCGD1	8503	8001	0.94
	SCG1.5	7984	5157	0.65
	SCGE1.5	7984	5921	0.74
	SCGD1.5	7984	8213	1.03
	SCG2	5012	3825	0.76
	SCGE2	5012	4080	0.81
	SCGD2	5012	4845	0.97
Average				0.83
Coefficient of Variation (COV)				0.15

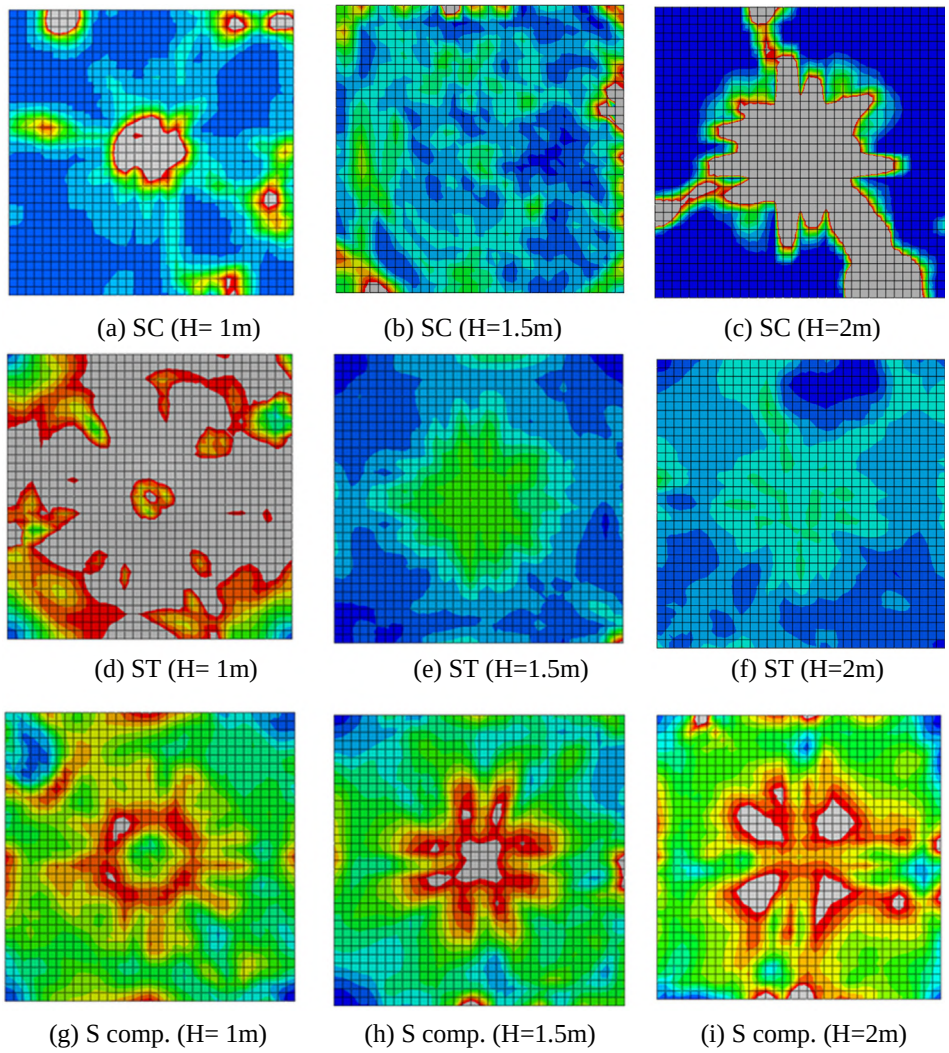


Fig. 18. Selected failure patterns obtained from numerical simulation based on ABAQUS package for un-strengthened, strengthened at tension side and strengthened at compression side specimens.

stiffness stage to no stiffness is defined as damage evolution ($D = 0$ to $D = 1$).

The simulation was designed to provide an alternate means to represent the drop weight impact. During an impact analysis, elements near the impact zone typically experience large amounts of deformation. The reduced characteristic lengths of these elements result in a smaller global time increment. Scaling the mass of these elements as required throughout the simulation can significantly decrease the computation time. Thus, variable mass scaling was used to scale the mass of elements periodically during each analysis step. To use this type of mass scaling, a desired minimum stable time increment was defined. Mass scaling factors were calculated automatically and applied, as required, throughout the step. The formulation of velocity (v) used in the model can be defined as follows:-

$$v = \sqrt{2gh} \tag{3}$$

4.1. Crack patterns and failure modes

All test slabs were simulated numerically under the effect of drop weight falling from a height (h) with prescribed velocity as obtained from Eq. (3). It is worth mentioning that the interface between the substrate slab and the SHCC layer was considered as complete bond. That is to verify the adequacy of the adopted surface preparation condition and show that which one is more close to be complete bond condition. Fig. 18 shows selected images for the developed maximum principle stresses developed at the failure state that comply with the cracking pattern obtained from the experimental tests as presented in Figs. 5–11.

4.2. Energy balance

In ABAQUS/Explicit, the energy balance equation for the entire model can be defined according to Eq. (4).

$$E_{total} = E_I + E_v + E_{FD} + E_{KE} - E_w = constant \tag{4}$$

where E_{total} is the total energy for the entire model, E_I is the internal energy, E_V is the viscous energy dissipated by damping mechanisms including bulk viscosity damping and material damping, E_{FD} is the friction energy dissipation, E_{KE} is the kinetic energy and E_W is the work done by externally applied loads. In general, the total energy (E_{total}) of any system remains constant since the energy cannot disappear only it can be transformed. Therefore, check the total energy

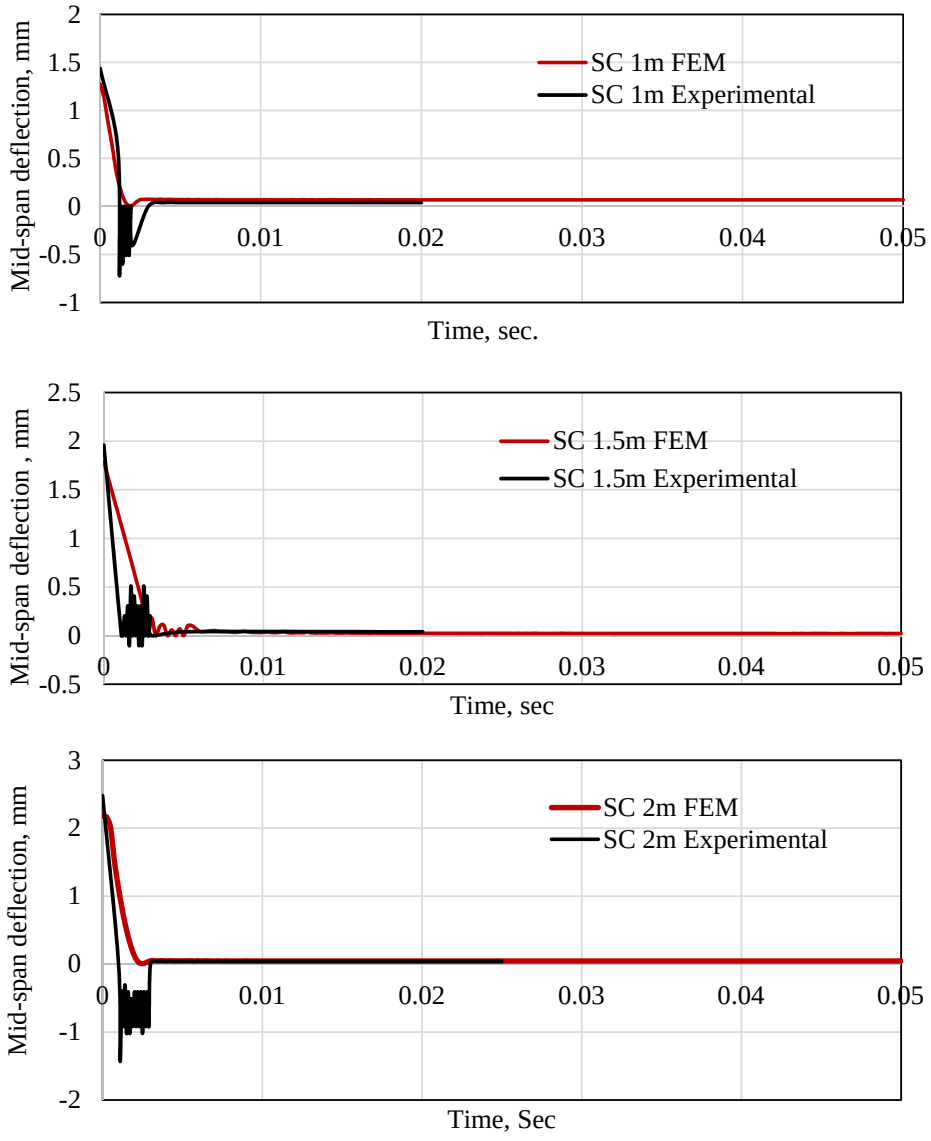


Fig. 19. Experimental maximum mid-span deflection versus time history against numerical simulation of all specimens of group I.

of the system is a good way to verify the stability of the analysis. In numerical analysis, the total energy is not completely constant and varies with time. ABAQUS specifies an error limit of 1% in total energy variation throughout the time duration to accept the stability of solution [30]. In addition, to monitor the total energy-time history, it is important to obtain different components of the internal energy as given by Eq. (5). The internal energy (E_I) is equal to the summation of recoverable elastic strain energy (E_E), the energy dissipated through inelastic plasticity processes (E_P), the energy dissipated through viscoelasticity or creep (E_{CD}), and the artificial strain energy or hourglass energy (E_A). The artificial energy is another useful quality check. It should be minimal, typically not exceed 5% of internal energy [30]. Large values of artificial strain energy indicate that mesh refinement is necessary.

$$E_I = E_E + E_P + E_{CD} + E_A \quad (5)$$

All components of energy can be easily obtained for all slabs numerically; however, the only component that can be verified against the experimental results is the kinetic energy. Thus, comparisons have been made between the experimental and numerical kinetic energies for all specimens as summarized in Table 5. It can be noticed that the numerical simulations gave comparable results to the experimental results with an average value of about 83%. The numerical results were obtained based on complete bond between the substrate slab and the SHCC layer. The comparison also showed that the numerical results of all slabs provided by SHCC layer at the tension side are very close to the slabs whose surface preparations were performed by grinding plus epoxy adhesive. This observation is in complete agreement with the experimental results where the slabs prepared by grinding plus epoxy adhesive exhibited the uppermost impact resistance among all slabs provided by SHCC layer at the tension side. Similarly, the numerical results confirmed that the surface preparation prepared by grinding plus shear dowels showed the highest impact resistance for all slabs provided by SHCC layers the compression side.

4.3. Maximum mid-span deflection-time history response

Based on the results of kinetic energy, the mid-span deflection-time history responses obtained from both experimental and numerical simulation were compared for the control unstrengthened slabs, SHCC-strengthened slabs at tension side based on grinding plus epoxy adhesive and SHCC-strengthened slabs at compression side based on grinding and steel dowels. Figs. 19–21 show experimental maximum mid-span deflection versus time history against numerical simulation results of all specimens of

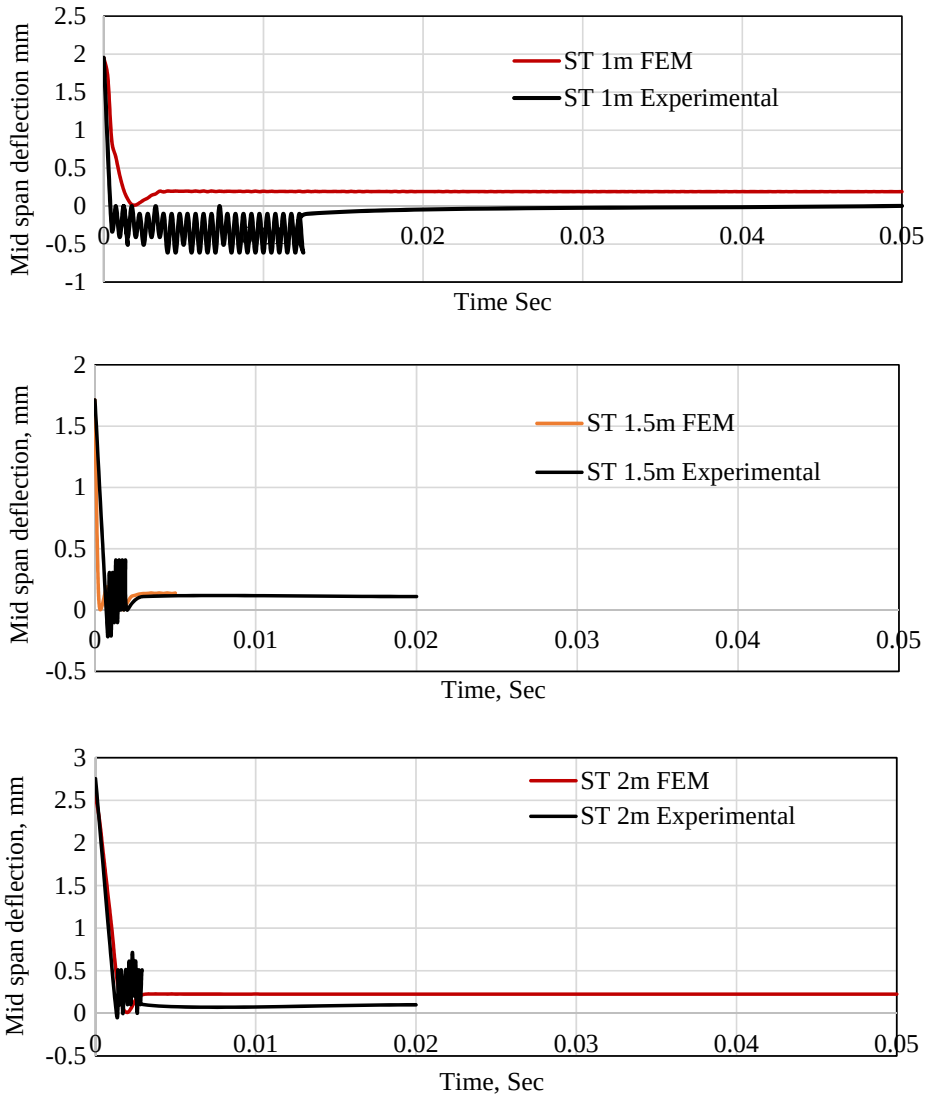


Fig. 20. Experimental maximum mid-span deflection versus time history against numerical simulation of all specimens of group II.

groups I, II and III, respectively. Comparisons show that the numerical simulation can properly predict the mid-span deflection-time history response for all specimens either un-strengthened or SHCC-strengthened specimens.

4.4. Numerical results of impact load

Another benefit of the numerical simulation is that the impact force as well as the total reaction force can be determined accurately for all specimens as depicted in Figs. 22–24. Generally, the model accurately estimates the time histories for all responses in terms of peak magnitudes and time responses. The obtained impact force and reaction force–time history under the effect of drop weight impact loading were found to be similar to those obtained experimentally by other researcher [43]. Typically, a time lag between the maximum impact force and the maximum reaction force was noticed for all un-strengthened and SHCC-strengthened slabs. This time lag is owing to the stress wave propagation travel from the impacted zone to the supports where this observation was also documented by other researchers [44–46].

Based on the numerical results, the average impact force that could trigger the failure of un-strengthened slabs was about 50 kN, while the average total reaction force was about 40 kN. Obviously, the maximum impact force is greater than that of the reaction force. The reason is that a part of the impact force is used to balance the inertial force, while the reaming portion of impact force is used to deform and fracture the test slab [46]. As for the SHCC-strengthened slabs at the tension side, the average impact force was about 119 kN, while the average reaction force was about 107 kN. Similarly, for the SHCC-strengthened slabs at the compression side, the average impact force was about 75 kN, while the average reaction force was about 62 kN. That means providing the SHCC layer at the tension side is better than adding the same layer at the compression side from the viewpoint of the ultimate load as well as reducing the impact effect on the SHCC-strengthened slabs.

5. Slabs subjected to incremental static loading

Based on the numerical results of the impact loads that triggered the complete failure of all slabs, 7 slab specimens were tested under the effect of incremental patch load applied at the central point of the slab over a contact area similar to that of the drop-weight. That is to obtain the failure load for such slabs under the effect of static loading. The test slabs consisted of one control un-strengthened slab and six strengthened slabs by SHCC layer

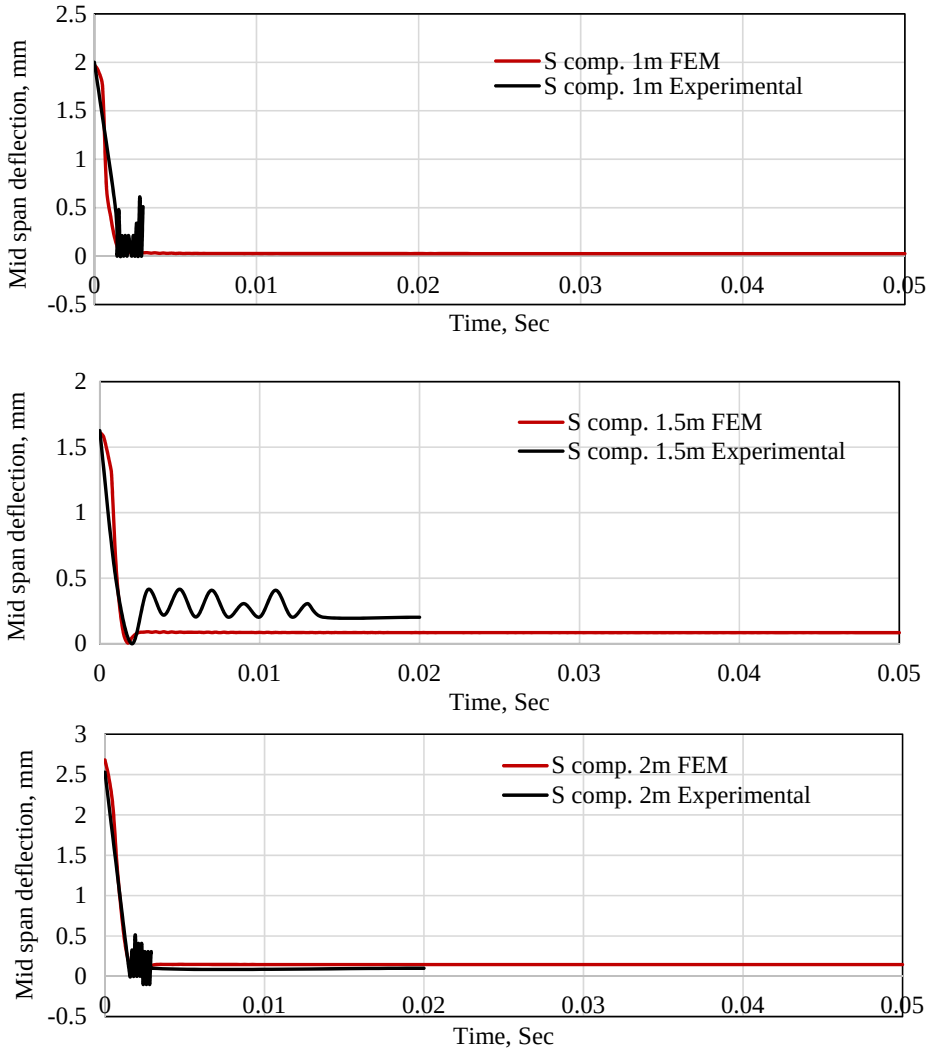


Fig. 21. Experimental maximum mid-span deflection versus time history against numerical simulation of all specimens of group III.

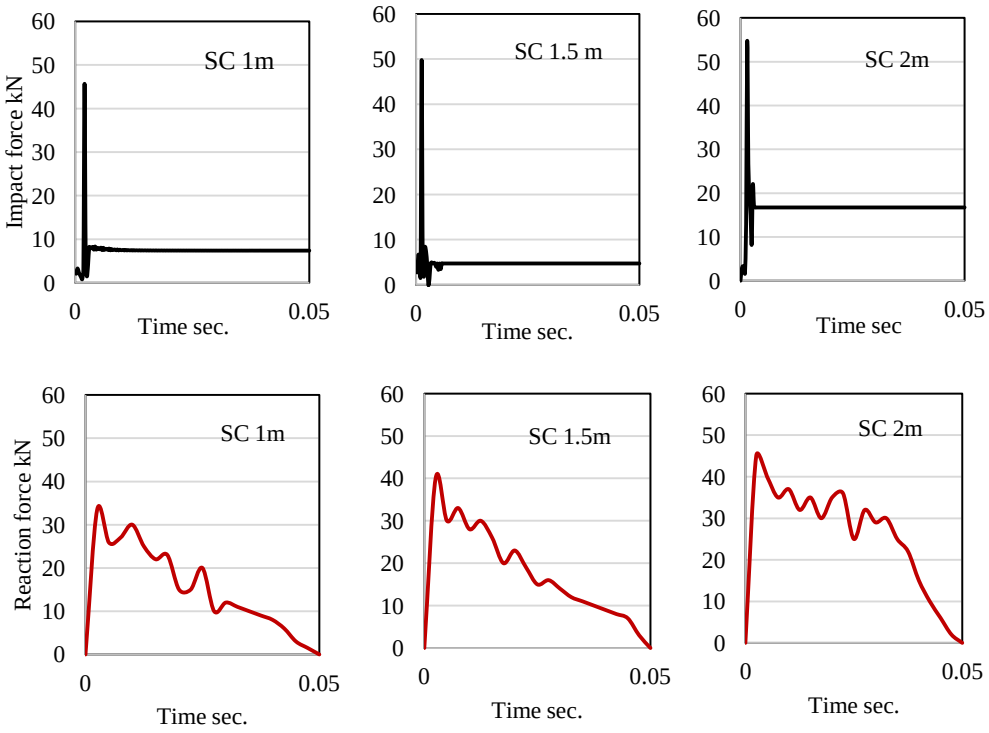


Fig. 22. Impact and reaction forces for all specimens of group I.

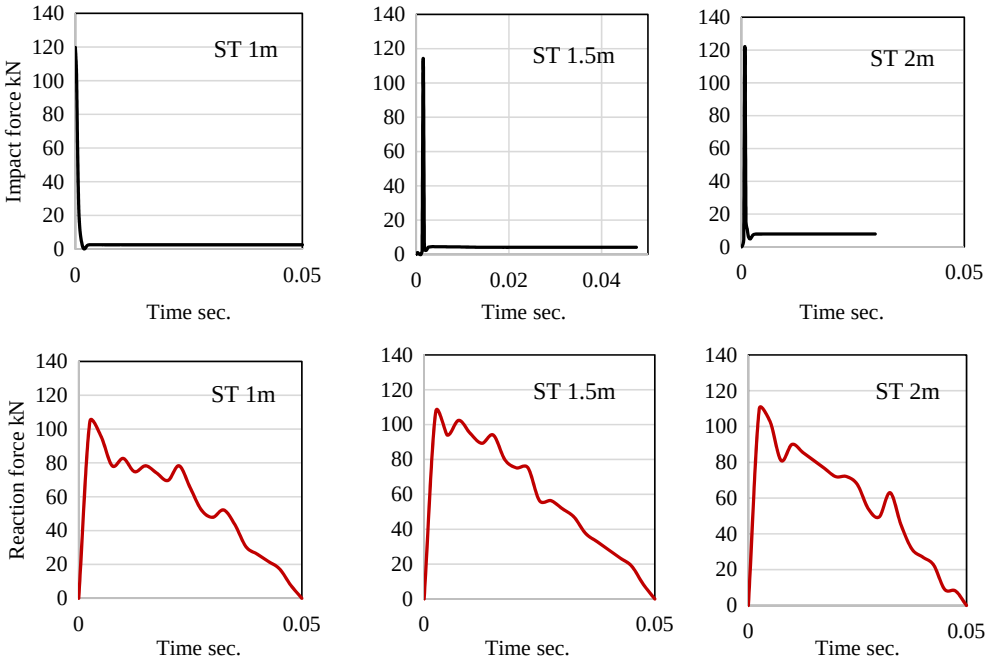


Fig. 23. Impact and reaction forces for all specimens of group II.

divided into two groups. Each group contained three slabs strengthened at either tension or compression side considering the three surface preparation techniques; namely, grinding (G), grinding plus epoxy (GE), and grinding plus steel dowels (GD).

The recorded ultimate load of the control slab SC was about 28 kN, while the recorded ultimate loads for slabs strengthened at tension side were about 104, 109, and 109 kN, respectively for slabs STG, STGE and STGD. Thus, both preparation techniques based on GE and GD are similar and showed the most significant enhancement in the ultimate capacity. Applying the SHCC layer at the compression side did not enable the strengthened slabs to sustain higher loads compared to those of strengthened slabs at the tension side. The recorded ultimate loads for slabs strengthened at compression side were about 62, 62, and 65 kN, respectively for slabs SCG, SCGE and SCGD. Thus, the strengthened slab adopted the preparation surface technique based on grinding plus

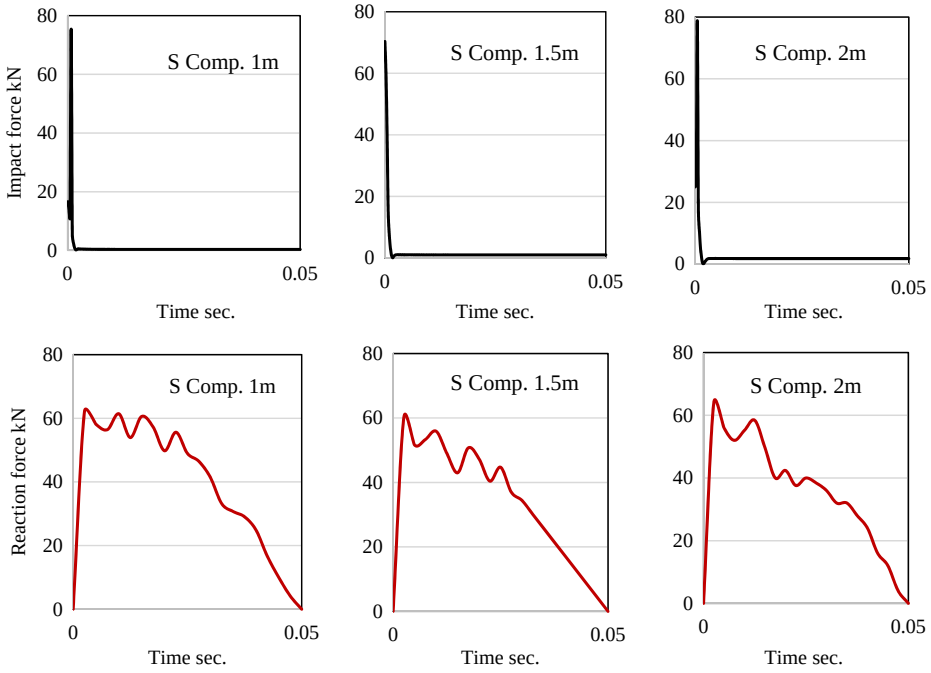
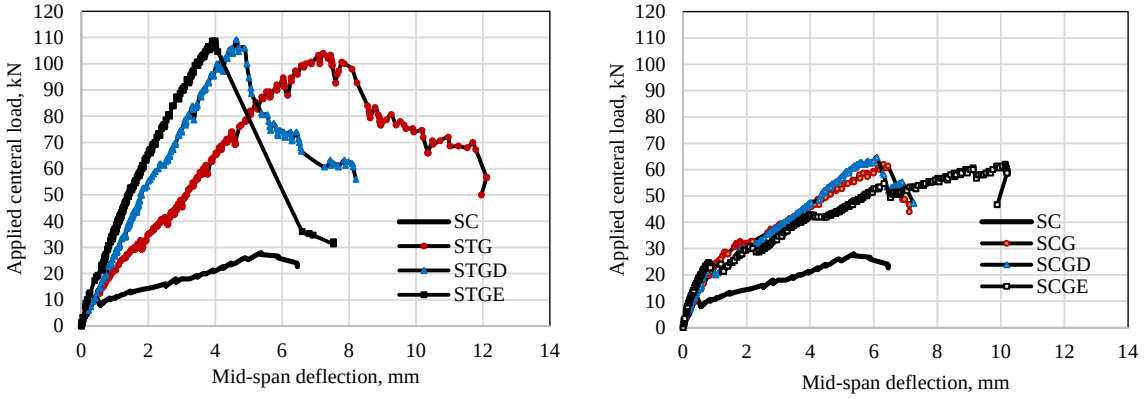


Fig. 24. Impact and reaction forces for all specimens of group III.

steel dowels (GD) enabled the strengthened slab SCGD to exhibit the most enhanced ultimate capacity.

Fig. 25(a) shows the relationship between the central mid-span deflection and the central patch load for all strengthened slabs by SHCC layer at the tension side. At the beginning of loading, the strengthened slabs showed slight decrease in the developed deflection owing to the increase in the flexural stiffness due to the increased overall depth. With further loading, the stiffness of the control slab SC degraded significantly due to the developed tensile cracks, while the strengthened slab showed smaller stiffness degradation owing to the enhanced tensile characteristics of the SHCC layer. However, the surface preparation technique affected the stiffness degradation rate. At the same loading level till the ultimate load, the slab STGE adopted grinding plus epoxy technique exhibited the lowest central deflection while the slab STG adopted the grinding technique only showed the highest central deflection. After reaching the ultimate load, the ultimate capacity showed some softening plateau owing to the developed softening plateau of the SHCC layer. However, the slab STGE showed sudden drop which could be attributed to the epoxy fracture. As for slabs strengthened at the compression side, Fig. 25(b) shows the relationship between the central mid-span deflection and the central patch load for all strengthened slabs. It can observed that (after cracking) at the same loading level, the surface preparation condition affect slightly the central deflection, however, in such configuration, the slab SCGE showed the highest mid-span deflection. For such slab, several kinks were noticed along the entire load-deflection plateau owing to the separation of the epoxy resin at the interface between the substrate slab and the SHCC overlay.

It can be concluded that adding the SHCC strengthening layer at the tension side enabled the strengthened slab to show higher ultimate capacity and lower mid-span deflection than those of the strengthened slab at the compression side as reported by others [23–25]. In addition, the surface preparation technique affected



(a) Slabs strengthened at tension side (b) Slabs strengthened at compression side

Fig. 25. Applied central load versus mid-span deflection for all slabs under the effect of incremental static loading.

the ultimate capacity slightly; however, it showed obvious effect on the exhibited central deflection.

6. Conclusion

Based on the considered concrete dimensions along with the internal reinforcement for both the substrate slabs and the SHCC overlay considering the adopted loading protocols, the following conclusions maybe drawn:

1. Owing to the enhanced impact resistance of the SHCC material, the sustained numbers of impact blows of the strengthened slabs were extremely higher than those sustained by the control un-strengthened slabs. However, the slabs provided by SHCC layers at the tension sides sustained higher impact blows than those sustained by the opponent slabs strengthened by SHCC layers at the compression side taking into account the surface preparation conditions as well as the height of the drop weight. Slabs STG1, STGE1 and STGD1 sustained numbers of blows corresponding to 3.5, 4.7 and 4 times the numbers sustained by the control slab SC1. On the other hand, the opponent values for slabs SCG1, SCGE1 and SCGD1 are 2.7, 2.9, and 3.5, respectively.
2. Increasing the drop height showed significant increase of the sustained blows for slab strengthened at the tension side, while it showed slight decrease for slab strengthened at the compression side. Slabs STG2, STGE2 and STGD2 sustained numbers of blows corresponding to 6.8, 8.2 and 6.2 times the numbers sustained by the control slab SC2. On the other hand, the opponent values for slabs SCG2, SCGE2 and SCGD2 are 2.5, 2.7, and 3.2, respectively.
3. The surface preparation technique showed significant effect of the impact resistance of the SHCC-strengthened slabs. For SHCC-strengthened slabs at tension sides, the surface preparation technique based on grinding plus epoxy adhesive enabled the strengthened slab to show the most enhanced impact resistance. On the other hand, the surface preparation technique based on grinding plus steel dowels enabled the strengthened slab at the compression side to exhibit the highest impact resistance.
4. Strengthening of RC slabs by SHCC layers at the tension sides enabled the strengthened slabs to develop higher impact ductility than those exhibited by strengthened slabs by SHCC layers at the compression sides. For slabs strengthened by SHCC layers at the tension side, the ductility indices for slabs STGE1, STGE1.5 and STGE2 were about 4.7, 7.3 and 8.2 times those of slabs SC1, SC1.5 and SC2, respectively. On the other hand, the ductility indices for slabs SCGD1, SCGD1.5 and SCGD2 were about 3.5, 4.3 and 3.2 times those of slabs SC1, SC1.5 and SC2, respectively.
5. From the kinetic energy viewpoint, the numerical results of all slabs provided by SHCC layers at tension sides were very close to the experimental results of slabs whose surface preparations were performed by grinding plus epoxy adhesive. This means that the surface condition prepared by grinding plus epoxy adhesive is the closest simulation to the complete bond condition. Similarly, the numerical results confirmed that the contact surface prepared by grinding plus shear dowels showed the closest simulation for the complete bond condition for all slabs provided by SHCC layers the compression side.
6. The average impact failure loads obtained numerically were about 50, 119 and 75 kN, respectively, for un-strengthened slabs, SHCC-strengthened slabs at tension side and SHCC-strengthened slabs at compression side. While, the corresponding average reaction forces were about 40, 107 and 62 kN, respectively. Thus, 25%, 11% and 21%. of the impact forces were used to balance the inertial force, while 75%, 89% and 79% of the impact forces were used to deform and fracture the test slabs. Therefore, the SHCC-strengthened slabs at either tension or compression side showed lower dynamic effect compared to that of un-strengthened slabs. However, the strengthened slabs at the tension sides showed lower dynamic effect compared to the slabs strengthened at the compression sides.
7. For both drop weight test and static loading test, adding the SHCC strengthening layer at the tension side enabled the strengthened slab to show higher ultimate capacity and lower mid-span deflection than those of the strengthened slab at the compression side. Besides, both tests confirmed that the surface preparation technique based on grinding plus epoxy adhesive enabled the strengthened slab at the tension side to show the most enhanced performance. In a similar way, both of them confirmed that the surface preparation technique based on grinding plus steel dowels is the best one for strengthened slab by SHCC layer at the compression side.

Declaration of Competing Interest

The authors declare no potential conflicts of interest with respect to the research, authorship and publication of this paper.

References

[1] K. Fujikake, B. Li, S. Soeun, Impact response of reinforced concrete beam and its analytical evaluation, J. Struct. Eng. 135 (8) (2009) 938–950.
[2] M. Verma, P.R. Prem, J. Rajasankar, B.H. Bharatkumar, On low-energy impact response of ultra-high performance concrete (UHPC) panels, Mater. Des. 92 (2016) 853–865.
[3] H. Othman, H. Marzouk, Performance of UHPFRC plates under repeated impact load, in: First International Interactive Symposium on UHPC, 2016, pp. 1–8.
[4] H. Habel, P. Gauvreau, Response of ultra-high performance fiber reinforced concrete (UHPFRC) to impact and static loading, Cem. Concr. Compos. 30 (2008) 938–946.
[5] E. Parant, P. Rossi, E. Jacquelin, C. Boulay, Strain rate effect on bending behavior of new ultra-high-performance cement-based composite, ACI Mater. J. 104 (2007) 458–463.
[6] P. Máca, R. Sovják, T. Vavříník, Resistance of ultra high performance fibre reinforced concrete to projectile impact, WIT Trans. State Art Sci. Eng. 75 (2014) 97–108.
[7] D. Elavarasi, R.K. Saravana, On low-velocity impact response of SIFCON slabs under drop hammer impact loading, Constr. Build. Mater. 160 (2018) 127–135.
[8] K.H. Mo, S.P. Yap, U.J. Alengaram, Z.J. Mohd, C. Hooi, Impact resistance of hybrid fibre-reinforced oil palm shell concrete, Constr. Build. Mater. 50 (2014) 499–507.
[9] A.I. Al-Hadithi, A.T. Al Ejbari, G.S. Jameel, Behavior of waste plastic fiber concrete slabs under low velocity impact, Iraqi J. Civil Eng. 9 (1) (2016) 135–148.
[10] V. Kumara, M.A. Iqbala, A.K. Mittalb, Impact resistance of prestressed and reinforced concrete slabs under falling weight indenter, Procedia Struct. Integrity 6 (2018) 95–100.
[11] V. Kumara, M.A. Iqbala, A.K. Mittalb, Energy absorption capacity of prestressed and reinforced concrete slabs subjected to multiple impacts, Procedia Struct. Integrity 6 (2017) 11–18.
[12] R. Ranade, V.C. Li, W.F. Heard, B.A. Williams, Impact resistance of high strength-high ductility concrete, Cem. Concr. Res. 98 (2017) 24–35.
[13] J. Wu, X. Liu, H. Zhou, L. Li, Z. Liu, Experimental and numerical study on soft-hard-soft (SHS) cement based composite system under multiple impact loads, Mater. Des. (2017) 1–73.
[14] J. Wu, S.H. Chew, Field performance and numerical modeling of multi-layer pavement system subject to blast load, Constr. Build. Mater. 52 (2014) 177–188.
[15] Pedro M.D. Santos, Eduardo N.B.S. Júlio, A state-of-the-art review on roughness quantification methods for concrete surfaces, Constr. Build. Mater. 38 (2013) 912–923.
[16] A. Garbacz, M. Górka, L. Courard, Effect of concrete surface treatment on adhesion in repair systems, Mag. Concr. Res. 52 (2004) 1–12.
[17] Andrzej Garbacz, Luc Courard, Katarzyna Kostana, Characterization of concrete surface roughness and its relation to adhesion in repair systems, Mater. Charact. 56 (2006) 281–289.
[18] J.G. Teng, T. Yu, D. Fernando, Strengthening of steel structures with fiber-reinforced polymer composites, J. Constr. Steel Res. 78 (2012) 131–143.
[19] H. Totanji, G. Ortiz, The effect of surface preparation on the bond interface between FRP sheets and concrete members, Compos. Struct- 53 (2001) 457–462.

[20] John J. Myers, Jason Jeffries, Xianlin Shen, Effect of varied surface roughness and concrete strength on the bond performance of FRP fabrics, in: Proceedings of ACIC 07 Advanced Composites in Construction, 2007, pp. 1–10.
[21] H.M. Afefy, N. Kassem, M. Mahmoud, S. Taher, Efficient strengthening of opened-joint for reinforced concrete broken slabs, Compos. Struct. 136 (2016) 602–615.
[22] A.B. Elnagar, A.T. Baraghith, H.M. Afefy, M.H. Mahmoud, Effect of internal reinforcement on the tensile characteristics of the UHP-SHCC Material, International Conference on Advances in Structural and Geotechnical Engineering, ICASGE'17, Hurghada, Egypt, 27-30 March, 2017.
[23] H.M. Afefy, T.M. Fawzy, Strengthening of RC one-way slabs including cut-out using different techniques, Eng. Struct. 57C (2013) 23–36.
[24] H.M. Afefy, M. Hussein, Structural performance of RC slabs provided by pre-cast ECC strips in tension cover zone, Constr. Build. Mater. 65 (2014) 103–113.
[25] H.M. Afefy, N. Kassem, M. Hussein, Enhancement of flexural behavior of CFRP-strengthened reinforced concrete beams using engineered cementitious composites transition layer, Struct. Infrastruct. Eng. 11 (2015) 1042–1053.
[26] Z. Deng, J. Li, Mechanical behaviors of concrete combined with steel and synthetic macro-fibers, Int. J. Phys. Sci. 1 (2) (2006) 57–66.
[27] V. Mechtcherine, O. Millon, M. Butler, K. Thoma, Mechanical behavior of SHCC under impact loading, HPFRCC 6 (2012) 297–304.
[28] V. Mechtcherine, O. Millon, M. Butler, K. Thoma, Mechanical behaviour of strain hardening cement-based composites under impact loading, Cem. Concr. Compos. 33 (2011) 1–11.
[29] I. Curosu, V. Mechtcherine, D. Forni, E. Cadoni, Performance of various strain-hardening cement-based composites (SHCC) subject to uniaxial impact tensile loading, Cem. Concr. Compos. 102 (2017) 16–28.
[30] ABAQUS, ABAQUS Theory manual, version 6.12, Hibbitt, Carlsson and Sorenson, Inc., Pawtucket, RI, USA, 2012.
[31] Egyptian code for design and construction of reinforced concrete structures (ECP 203-2018), 2018.
[32] J. Sawan, M. Abdel-Rohman, Impact effect on RC slabs: Experimental approach, J. Struct. Eng. 112 (9) (1987) 2057–2065.
[33] S. Murtiadi, H. Marzouk, Behaviour of high-strength concrete plates under impact loading, Mag. Concr. Res. 53 (1) (2001) 43–50.
[34] A.M. Alhozaimy, P. Soroushian, F. Mizra, Mechanical properties of polypropylene fiber reinforced concrete and the effect of pozzolanic materials, Cem Concr Comp 18 (1996) 65–92.
[35] N. Wang, S. Mindess, K. Ko, Fiber reinforced concrete beams under impact loading, Cem. Concr. Res. 26 (1996) 363–376.
[36] H. Toutanji, S. McNeil, Z. Bayasi, Chloride permeability and impact resistance of polypropylene-fiber-reinforced silica fume concrete, Cem. Concr. Res. 28 (1998) 961–968.
[37] P.S. Song, S. Hwang, B.C. Sheu, Strength properties of nylon- and polypropylene-fiber-reinforced concretes, Cem. Concr. Res. 25 (2005) 1546–1550.
[38] T. Belytschko, W. Liu, B. Moran, Nonlinear Finite Elements for Continua and Structures, second ed., John Wiley & Sons Inc, West Sussex, England, 2014, p. 804.
[39] A. Chopra, Dynamics of Structures: Theory and Applications to Earthquake Engineering, fourth ed., Pearson Education Inc., New Jersey, USA, 2012, p. 944.
[40] A. Sangi, I. May, High-mass low-velocity impacts on reinforced concrete slabs, 7 European LS-DYNA Conference. Salzburg, Austria, 2009.
[41] O. Martin, Comparison of different constitutive models for concrete in ABAQUS/Explicit for missile impact analyses, JRC Scintific and Technical Reports, Luxembourg, 2010, 44 pp.
[42] N. Kishi, Y. Kurihashi, S. Ghadimi Khasraghy, H. Mikami, Numerical simulation of impact response behavior of rectangular reinforced concrete slabs under falling-weight impact loading, Appl. Mech. Mater. 82 (2011) 266–271.
[43] H. Othman, Performance of ultra-high performance fiber reinforced concrete plates under impact loads Ph.D Thesis, Civil Engineering Dept., Ryerson University, Toronto, ON, Canada, 2016.
[44] T. Hrynyk, F. Vecchio, Behavior of steel fiber-reinforced concrete slabs under impact load, ACI Struct. J. 111 (5) (2014) 1213–1224.
[45] S. Saatci, F. Vecchio, Effects of shear mechanisms on impact behavior of Reinforced Concrete Beams, ACI Struct. J. 106 (1) (2009) 78–86.
[46] S. Soleimani, N. Banthia, A novel drop weight impact setup for testing reinforced concrete beams, Exp. Tech. 38 (3) (2014) 72–79.